ACS APPLIED MATERIALS & INTERFACES

Research Article

www.acsami.org

Facile Hydrothermal Synthesis of Nanostructured Hollow Iron–Cerium Alkoxides and Their Superior Arsenic Adsorption Performance

Bo Chen,[†] Zhiliang Zhu,*[,†] Shuxia Liu,[†] Jun Hong,[†] Jie Ma,[†] Yanling Qiu,[†] and Junhong Chen*[,†,‡]

[†]State Key Laboratory of Pollution Control and Resource Reuse, College of Environmental Science and Engineering, Tongji University, 1239 Siping Road, Shanghai 200092, P. R. China

[‡]Department of Mechanical Engineering, University of Wisconsin–Milwaukee, Milwaukee, Wisconsin 53211, United States

Supporting Information

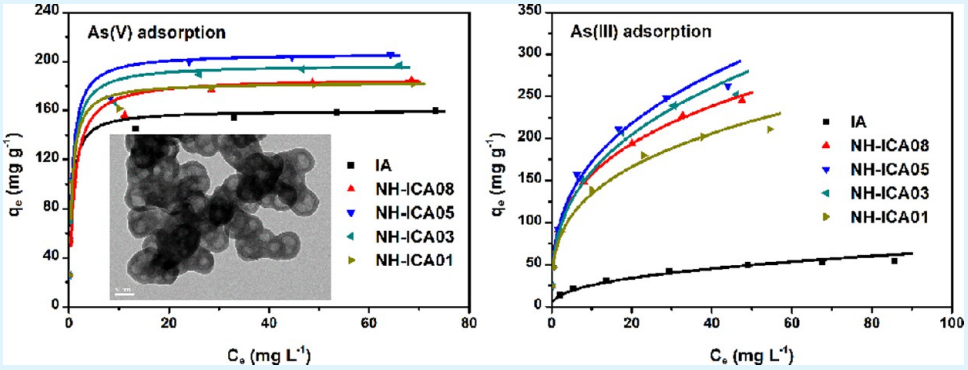

ABSTRACT: Recently, metal oxides with novel nanostructured architectures have been prepared by annealing the polyol-based metal alkoxides for water treatment. However, these materials often exhibit relatively low adsorption capacities possibly attributable to the decomposition of surface groups during the calcination process. In this work, we successfully synthesized a novel nanostructured hollow iron–cerium alkoxide (NH-ICA) with a high surface area and abundant surface functional groups through an ethylene glycol mediated solvothermal method. Cerium ion doping significantly influenced the morphologies, microstructures and adsorption performance of NH-ICAs. Interestingly, the synthesized NH-ICAs showed significantly higher affinity to As(III) than the iron alkoxide material without cerium doping. Moreover, a much higher adsorption capacity of the NH-ICAs for As(III) than As(V) was found. When the molar ratio of Fe to Ce was 5:1, the product with uniform nanostructured hollow architectures exhibited the best adsorption capacities for both As(V) and As(III) (206.6 and 266.0 mg g^{-1}, respectively). The mechanistic study revealed that As(V) adsorption involved ion-exchange between the As(V) species and three types of negatively charged groups, including surface hydroxyl groups, CO_3^{2-} and unidentate carbonate-like species. For As(III) adsorption, surface complexing was proposed. A broad adaptation pH range for both As(V) and As(III) adsorbed by the resulting product indicates its promising application perspective for decontamination of arsenic-polluted water.

KEYWORDS: *nanostructure, hollow, iron–cerium, alkoxides, arsenic, adsorption*

1. INTRODUCTION

Natural groundwater contaminated by arsenic has been an area of great concern throughout the world because of the hypertoxicity and serious side effects of arsenic. Therefore, efficient removal of arsenic from water has garnered significant attention in water treatment. World-wide researchers have exploited a large number of adsorbents to remove arsenic pollutants from water systems.[1−3] As is well-known, one of the most important requirements for an excellent adsorbent is a large interface for pollutants. Thus, the development of nanomaterials has attracted increasing attention because of their large surface area, abundant surface active sites, facile mass transportation, and many other interesting functions.[4−7] Iron hydroxide/oxide-based adsorbents have been the most popular candidates for arsenic removal, in view of their natural abundance, low-cost, eco-friendliness, and especially strong affinity to arsenic.[8−11] Currently, it has been reported that iron-containing nanomaterials (ICMs) with various novel morphologies and microstructures exhibit enhanced arsenic uptake properties compared with their bulk counterparts.[12] Recently, metal oxides with novel structures have been prepared by the calcination of polyols-based metal alkoxides.[5,13−15] For example, Zhong et al. synthesized flowerlike iron oxides using $FeCl_3{\cdot}6H_2O$ and urea by an ethylene glycol (EG)-mediated

Received: May 29, 2014
Accepted: August 5, 2014
Published: August 5, 2014

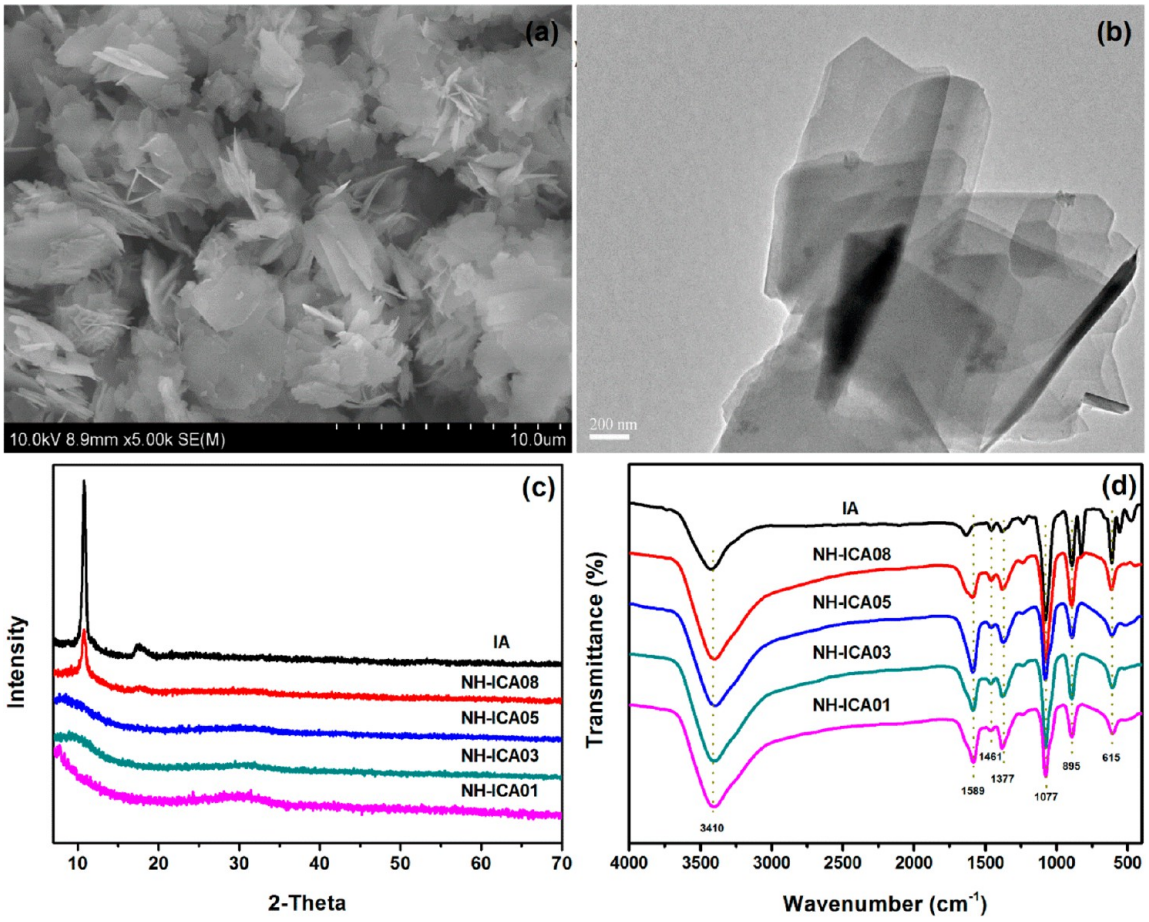

Figure 1. (a) SEM and (b) TEM images of IA; (c) XRD patterns and (d) FTIR spectra of IA, NH-ICA08, NH-ICAO5, NH-ICA03, and NH-ICA01.

process.[13] The iron oxides were obtained through the calcination of the precursor and subsequently used for wastewater treatment, and the maximum adsorption capacity of this material was 5.31 mg g^{-1} for arsenate. However, the arsenic adsorption abilities of these materials are still relatively low, which may be due to the decomposition of active groups on their surfaces by calcination. Moreover, tedious synthesis pathways and sometimes expensive chemicals were usually employed, which might limit their further practical use. Therefore, developing a facile method for synthesizing efficient ICMs for arsenic removal is highly desirable.

Furthermore, adsorption mechanisms for arsenic are very important for the rational structural design and fabrication of excellent adsorbents. Generally, the adsorption between adsorbents and arsenic are believed to be attributable to electrostatic attraction, surface complexation and/or ion-exchange with active functional groups on the surface of adsorbents. Heretofore, hydroxyl groups are widely considered as the surface active groups.[16,11,17−19] Thus, the adsorption efficiency of arsenic remarkably depended on the pH value of the solutions, resulting from the species transformation of arsenic at different pH as well as the protonation at a low pH value and the deprotonation at a higher pH value of surface hydroxyl groups. Recently, some groups developed surface-activated groups, such as carbonate, to improve arsenic uptake capacities.[20,21] In fact, it is scarcely possible to control the acidity or alkalinity of natural water systems. Thus, it is very important to develop an adsorbent with high arsenic removal efficiency under a broad pH range.

In this work, our objective was to synthesize an efficient ICMs material for arsenic removal with a simple method and a superior arsenic uptake capacity. Therefore, a novel nano-structured hollow iron−cerium alkoxide (NH-ICA) was synthesized using a solvothermal method mediated with EG. The obtained NH-ICAs were used as the adsorbents to remove As(V) and As(III) from water, and exhibited remarkable advantages with a superior arsenic adsorption capacity for arsenic and good adaptability under a broad pH range. The results showed that Ce doping in varying proportions could significantly change the morphology and the structure of iron alkoxide (IA). Plausible ion-exchange mechanisms were proposed for As(V) and As(III) adsorption, which are supported by Fourier transform infrared spectroscopy (FTIR), X-ray photoelectron spectroscopy (XPS), and other experimental results.

2. EXPERIMENTAL SECTION

2.1. Chemicals. The source and purity of the chemicals, the preparation of As(V) stock solution and working solutions, and the preparation of As(III) solutions were described in our previous work.[6] All the reagents were used without further purification.

2.2. Synthesis of Iron Alkoxide (IA). In a typical procedure, 1.1 g (4.08 mmol) $FeCl_3 \cdot 6H_2O$, 2.2 g (36.6 mmol) urea and 6 g (18.6 mmol) tetrabutylammonium bromide (TBAB) were dissolved in 180 mL EG in a 250 mL three-necked flask. The obtained red solution was magnetically stirred and heated to 180 °C by an automatic temperature control heating device. After refluxing for about 50 min minutes, the reaction mixture was naturally cooled to room temperature. The yellow-green precipitate was collected by

centrifugation and washed with ethanol several times, and finally dried at 80 °C overnight. The final solid was the iron alkoxide and named as IA.

2.3. Synthesis of NH-ICAs. All other synthesis conditions and procedures were similar to the preparation of IA with the exception of the metal salt precursors. Two salts including $FeCl_3 \cdot 6H_2O$ and $CeCl_3 \cdot 7H_2O$ with different molar ratios of 8:1, 5:1, 3:1 and 1:1, were used as the metal salt precursors. The total mole of the precursors was constant at 4.08 mmol. The obtained nanostructured hollow iron−cerium alkoxides materials were termed as NH-ICA08, NH-ICA05, NH-ICA03, and NH-ICA01, respectively, corresponding to the molar ratio.

2.4. Characterization. The synthesized products were characterized by field-emission scanning electron microscopy (SEM), transmission electron microscopy (TEM), X-ray diffraction (XRD), Fourier transform infrared absorption spectrometer (FTIR), thermogravimetric analysis (TGA), and X-ray photoelectron spectroscopy (XPS). All these apparatus models, manufacturers and test conditions were the same as those reported in our previous work.[6] Nitrogen adsorption/desorption isotherms were collected using an Autosorb-iQ of Quantachrome at 77 K, with degassing at 373 K prior to the measurements. Brumauer-Emmett-Teller (BET) method was utilized to calculate the specific surface areas. The cumulative pore volume and pore size distribution curves were estimated using nonlocal density functional theory (NLDFT) kernel. The residual arsenic in solutions was determined by an inductively coupled plasma optical emission spectrometry (ICP-OES, Agilent 720 ES, USA).

2.5. Adsorption Experiments. All the adsorption experiments were carried out in well-capped 150 mL flasks, containing 50 mL of solution with required arsenic concentrations. The flasks were then vibrated in a thermostatic shaker with the speed of 150 rpm·min^{-1} at 298 K. After a specified duration, the adsorbents were separated using a 0.45 μm filter membrane. Adsorption isotherms and kinetics were studied at pH 6 for As(V) and As(III). For the adsorption isotherm study, 10 mg adsorbents were added to 50 mL solution with arsenic concentrations ranging from 1 to 100 mg L^{-1} under stirring for 24 h, respectively. For the kinetic study, samples were collected at different intervals in arsenic solutions with the initial concentration of 20 mg L^{-1}. For the pH effect experiments, the initial pH values (pH_i) of the solutions range from 2 to 10 and the initial arsenic concentration of arsenic solution was 20 mg L^{-1}. The competitive experiments were carried out in 20 mg L^{-1} (0.267 mmol L^{-1}) arsenic solution at pH 6, containing 1.33 mmol L^{-1} of F^-, NO_3^-, SO_4^{2-}, CO_3^{2-}, SiO_3^{2-}, and PO_4^{3-}. The adsorbents loading with arsenic were obtained by filtration, subsequently washed with deionized water, and finally dried in a vacuum oven at 80 °C. All the experiments were repeated twice to ensure the reliability of experimental results in the present study.

3. RESULTS AND DISCUSSION

3.1. Characterizations. The morphology of IA observed by SEM and TEM are shown in Figure 1. The SEM image reveals that the typical product consists of 3D lamellar architectures with irregular distribution in sizes (Figure 1a). The entire structure of the architecture is built from several thin nanopetals with a smooth surface, which is consistent with the result of TEM imaging (Figure 1b). These nanopetals are only several nanometers thick and 2−4 μm wide, and connect to each other through the center to form the 3D structures. The powder X-ray diffraction (XRD) pattern of IA (Figure 1c) shows a very strong low-angle peak corresponding to interlayer spacing lamellar structure which is the characteristic of stacked metal−oxygen sheets separated by bonded alcoholate anions.[14,15] Although various organometallic precursors produced from these processes have been studied, detailed information on their crystal structures remains unclear.[22,23] Xia et al. proposed that this peak could be ascribed to the formation of glycolate originated from the coordination and alcoholysis of EG with metal ions.[24,25] There are no other obvious diffraction peaks, indicating the amorphous nature of obtained samples.

In the FTIR spectra (Figure 1d), the absorption bands centered at ~3410 and ~1600 cm^{-1} are attributed to the H−O−H bond stretching vibrations. According to the reported results, there were two types of carbonate groups produced by the hydrolysis of urea: (i) the bands at 1377 cm^{-1} can be assigned to CO_3^{2-};[20] (ii) the bands at 1461 and 895 cm^{-1} are associated with the vibrational mode of unidentate carbonate-like species, which was produced by the complexion between CO_3^{2-} and iron/cerium ions.[21,26−28] The intensive peak at 1077 and 615 cm^{-1} are attributed to the abundant surface hydroxyl groups (M−OH) and M-O (M represents Fe and Ce), respectively.[16,29] TGA-DSC analysis revealed the oxidation and decomposition behaviors of various composites in IA, as shown in Figure S1 in the Supporting Information. After the calcination in air, the weight content of iron oxide was 53.4%. The wide weight loss of 38.84 below ~200 °C resulted from the decomposition of adsorbed water and abundant surface hydroxyl groups, which was also consistent with the results of FTIR spectra. The weight loss between ~220 and ~450 °C could be related to the degradation of carbonate groups in IA. The N_2 adsorption/desorption isotherms and pore distribution curves are demonstrated in Figure 2. The BET specific surface area and the total pore volume were 30.57 m^2 g^{-1} and 0.075 cc g^{-1}, respectively. Pore size analysis indicates a wide pore size

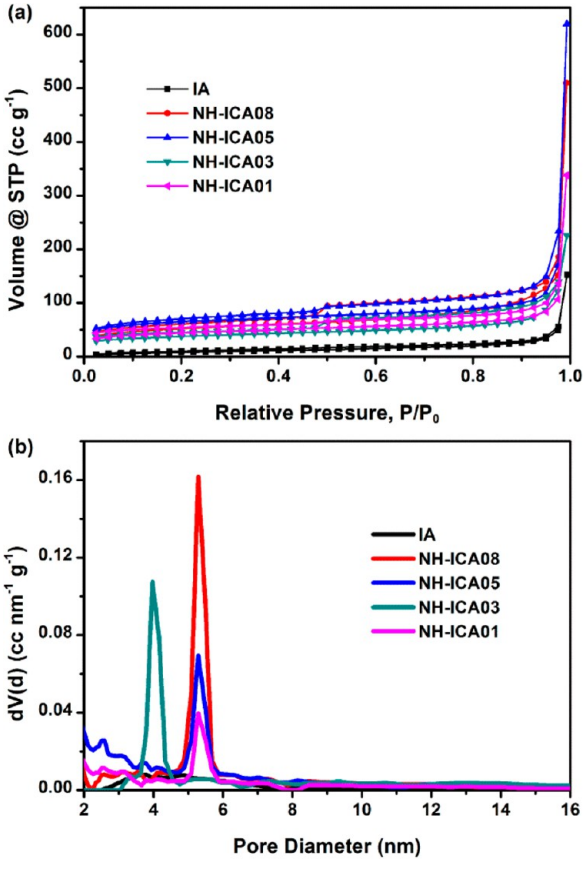

Figure 2. (a) N_2 adsorption/desorption isotherms and (b) pore size distribution curves of IA, NH-ICA08, NH-ICAO5, NH-ICA03, and NH-ICA01.

distribution of IA with an average pore size of 3.78 nm. The surface area and other porosity parameters are presented in Table 1.

Table 1. Surface Area and Porosity Parameters of As-Synthesized IA and NH-ICAs

samples	surface area $m^2\ g^{-1}$	total pore volume (cc g^{-1})	average pore size (nm)	cumulative mesopore (cc g^{-1})	cumulative micropore (cc g^{-1})
IA	30.57	0.075	3.78	0.056	0
NH-ICA08	170.2	0.234	5.28	0.168	0.042
NH-ICA05	217.5	0.262	5.29	0.176	0.050
NH-ICA03	124.7	0.188	3.97	0.136	0.045
NH-ICA01	144.3	0.165	1.78	0.096	0.054

To investigate the relative amount of mixed Ce on the product morphology, we conducted a series of experiments by varying the Ce content added in the reaction system while keeping other conditions unchanged. Interestingly, it was found that even a slight change in the Ce concentration can significantly affect the morphologies and microstructures. Images a and e in Figure 3 show the structure of NH-ICA08. No obvious lamellar structure in NH-ICA08 can be observed. The SEM image (Figure 3a) indicates the product is composed of nanoparticles or microspheres. The TEM image (Figure 3e) reveals the heterogeneous structure of NH-ICA08, with a small quantity of hollow architecture was formed in some regions. If the ratio of Fe to Ce ions decreased to 5:1, the resulting product contained uniform particles with noticeable uniform hollow structure (Figure 3b) confirmed by the TEM image. Figure 3f shows that the particle size of NH-ICA05 was ~120 nm and the walls thickness was 10 to 15 nm. When the initial concentration of iron ions continuously decreased to 3:1, most of the hollow structures remained with the appearance of some solid particles (Figure 3c). As can be confirmed from the TEM image (Figure 3g), novel heterogeneous structures were observed; the hollow structures became less pronounced and a small number of tiny nanoparticles are present inside or outside of the hollow particles. Otherwise, the wall thickness of NH-ICA03 also increased to 20−40 nm. Further increasing the initial concentration of Ce ions (NH-ICA01), the hollow interior completely disappeared and uniform solid nanoparticles formed with sizes of ~100 nm (Figure 3d, h).

The formation process of 3D hierarchical structured IA is conjectured to be consistent with previous reports of a two-stage self-assembly process, which involves a fast nucleation of amorphous primary particles followed by a slow aggregation and crystallization of primary particles.[13,30,31] However, many other factors such as crystal-face attraction, electrostatic and dipolar fields associated with the aggregate, van der Waals forces, hydrophobic interactions, and hydrogen bonds, may influence the self-assembly process.[13,32,33] When cerium ions were mixed, the morphologies and microstructures significantly changed. The aforementioned observations indicate that the formation of hollow interiors in as-prepared NH-ICAs depends primarily on the initial concentration ratio of Fe to Ce ions in the reaction system. The reason for the formation of hollow architectures by Ce doping may be due to Ostwald ripening.[34] The actual mechanism for the final nanostructured morphologies by assembling method is still a challenge in nanomaterial research.

The XRD patterns of NH-ICAs were further investigated to confirm the structure of the products, as shown in Figure 1c. The results indicate that the increase of initial cerium ion concentrations resulted in obviously weakened peaks at ~10°, indicating more Ce addition led to a less pronounced hierarchical structure. When the initial concentration ratio of Fe to Ce ions decreased to 5:1, the peak almost completely disappeared, indicating the absence of a hierarchical structure in NH-ICA05. XRD results are consistent with the SEM and TEM analyses. FTIR spectra of NH-ICAs indicate that the Ce addition could affect the number of surface functional groups (Figure 1d). The bands at 895, 1077, and 1461 cm^{-1} slightly changed, demonstrating the Ce ion doping would not have an noticeable effect on the number of surface hydroxyl groups and unidentate carbonate-like species. The intensity of the bonds at 1377 cm^{-1} is obviously enhanced, whereas the stretching vibration at 615 cm^{-1} clearly weakened, which indicates that the Ce ion doping resulted in more CO_3^{2-} groups and less M-O in the products. On the other hand, the specific surface area and pore size distribution of as-synthesized NH-ICAs were studied, as shown in Figure 2. It can be clearly found that the Ce doping can significantly increase the specific surface area and total pore volume of IA. The surface area significantly increased with the increase of the relative Ce content until the ratio of Fe to Ce ions reached 5:1 (217 $m^2\ g^{-1}$), which is due to the distinctly increasing volume of cumulative mesopores and micropores resulting from the formation of uniform hollow architectures. The continuous increase of Ce contents resulted in the surface area decrease, attributing to the decrease in the volume of cumulative mesopores caused by the gradual disappearance of hollow interiors. The higher surface area and the smaller average pore size of NH-ICA01 than those of NH-ICA03 are due to more micropores present in NH-ICA01. These results are quite consistent with the information obtained from SEM and TEM images.

3.2. Arsenic Adsorption Property. On the basis of the novel hollow structure, abundant surface functional groups, large surface areas and high porosity, the prepared NH-ICAs are promising as adsorbents for the decontamination of pollutants in water systems. The adsorption capacity of as-prepared IA and NH-ICAs was evaluated using the equilibrium adsorption isotherms fitted by varying initial concentrations of arsenic. Two classical equations, Langmuir and Freundlich models, were used to fit the experimental data. The mathematical expressions can be represented in a linear form and have been described with great details in our previous work.[35]

The amounts of adsorbed arsenic versus the corresponding aqueous-phase equilibrium concentration have been plotted as adsorption isotherms in Figure 4. The adsorption of As(V) by IA and NH-ICAs fit the Langmuir model better, indicating the adsorption process as a more likely monolayer adsorption process on a homogeneous surface. On the contrary, the adsorption of As(III) could be better fitted by the Freundlich model, which suggests the adsorption process is a multilayer adsorption process on a homogeneous surface.[36] The difference in sorption behaviors may be due to the different distribution of As(V) and As(III) species under the experimental pH conditions.[35] As(V) existed mainly as $H_2AsO_4^-/HAsO_4^{2-}$; therefore, an electrostatic effect between As(V) species and surface charged adsorbents occurred. However, As(III)

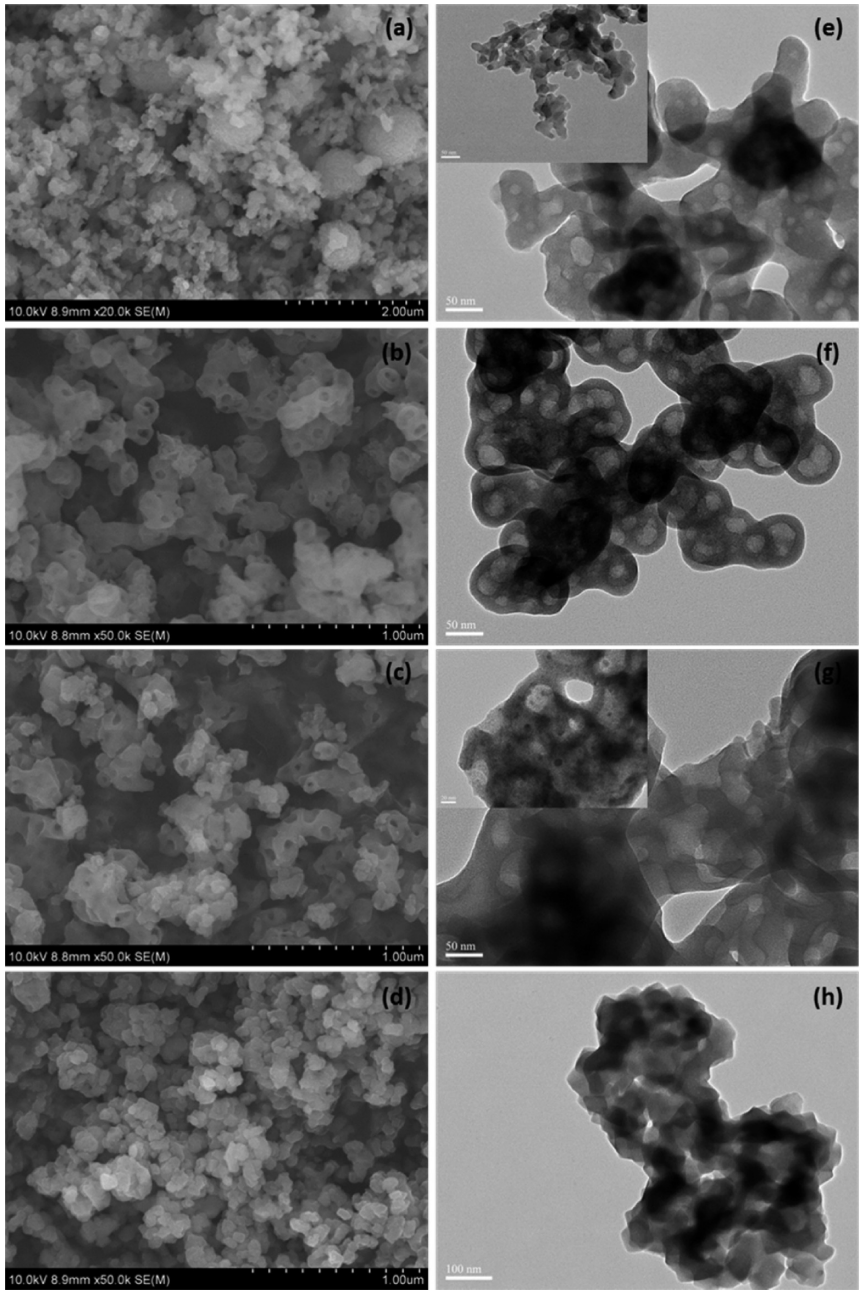

Figure 3. SEM images and TEM images of (a, e) NH-ICA08, (b, f) NH-ICA05, (c, g) NH-ICA03, and (d, h) NH-ICA01. The insets of e and g are the different areas of as-prepared products.

predominantly existed as H_3AsO_3.[37] Little electrostatic interaction existed between As(III) species and the adsorbents so that the As(III) adsorption should continue to increase with the increase of As(III) concentration.[36,38] The maximum adsorption capacities of IA for As(V) and As(III) were 160.2 and 58.79 mg g^{-1}, respectively. The great difference in the adsorption capacities between As(V) and As(III) by IA might be due to their different adsorption mechanisms. It can be clearly found from Figure 4 that the Ce doping can significantly enhance the adsorption capacity for arsenic, especially for As(III). The calculated isotherm parameters of the adsorbents for arsenic are summarized in Table S1 in the Supporting Information. The results show that NH-ICAs exhibited slightly enhanced As(V) removal capacities while a significant enhancement for As(III) adsorption was observed. NH-ICA05 exhibited the highest capacities for both As(V) and As(III) (206.6 and 266.0 mg g^{-1}, respectively). It may be associated with the synergistic effect of its abundant surface functional groups and the large number of uniform hollow architectures. Additionally, the maximum As(V) and As(III) adsorption capacities for NH-ICA08, NH-ICA03 and NH-ICA01 were calculated to be 186.3 and 247.8 mg g^{-1}, 197.2 and 256.7 mg g^{-1}, and 183.1 and 213.2 mg g^{-1}, respectively. NH-ICAs exhibited slightly enhanced As(V) adsorption, indicating the As(V) adsorption does not depend on the structures of the adsorbents but possibly depends on the surface functional groups, which will be discussed subsequently. However, the larger surface area and pore volume attributing to the formation of the nanostructured hollow architectures might be responsible for the great enhancement for As(III) adsorption. NH-

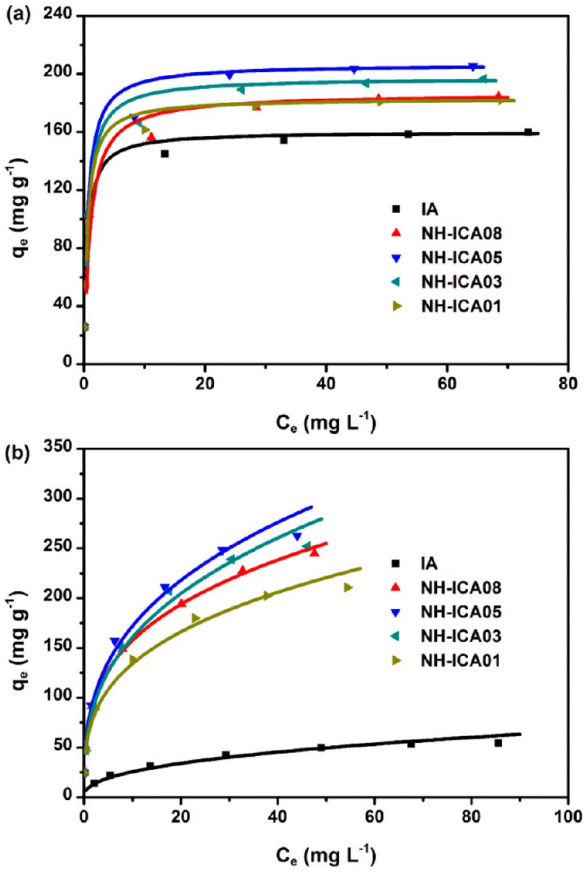

Figure 4. Adsorption isotherms of (a) As(V) fitted by the Langmuir model and (b) As(III) by the Freundlich model, respectively, on IA and NH-ICAs. The initial arsenic concentration ranged from 1 to 100 mg L^{-1}. The dosage of adsorbents and the initial pH value were 0.2 g L^{-1} and 6, respectively.

ICA03 possessed the lowest surface area; however, it exhibited higher As(III) removal capacity than NH-ICA08 and NH-ICA01. This reasonably suggests the higher BET surface area is not the only criterion for the high As(III) adsorption capacities by NH-ICAs, which are sometimes also influenced by the surface properties.[36] To evaluate the arsenic adsorption performance of the nanostructured hollow NH-ICA05, the adsorption capacity of NH-ICA05 was compared with other reported metal oxide micro-/ nanostructures (Table 2). The results indicated that the NH-ICA05 in this study exhibited a higher adsorption capacity for arsenic than those in the reported literatures.

The amount of arsenic removal by the NH-ICA05 as a function of time was studied, as shown in Figure 5a. The whole

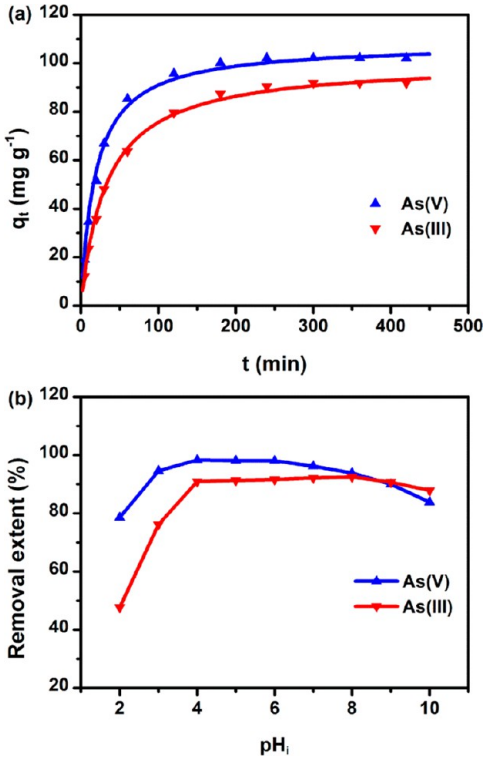

Figure 5. Arsenic adsorption on NH-ICA05 as a function of (a) time fitted by pseudo-second-order model and (b) pH values. The initial arsenic concentration and the dosage of adsorbents were 20 mg L^{-1} and 0.2 g L^{-1}, respectively, for both As(V) and As(III) adsorption. The initial pH of the solution for kinetic studies was 6 for As(V) and As(III).

Table 2. Comparison of BET Surface Area and the Adsorption Capacity of Arsenic on NH-ICA05 with Other Reported Materials

adsorbents	BET surface area (m^2 g^{-1})	pH		adsorption capacity (mg g^{-1})		ref
		As(V)	As(III)	As(V)	As(III)	
NH-ICA05	217.5	6	6	206.6	266.0	this study
$Al(OH)CO_3$	484	7		170		20
$Ni_2CO_3(OH)_2$	154.5			49.6		21
Porous Fe_3O_4	32.75	5 ± 0.2	5 ± 0.2	7.23	6.77	36
Flowerlike α-Fe_2O_3	40	4		5.31		13
3D CuO	119		5 ± 0.2		>12.9	5
hollow ceria	72	3		22.4		34
Fe–Mn binary oxide	265	5 ± 0.1	5 ± 0.1	69.75	132.75	39
iron(III)–copper(II) oxide	282	7.0	7.0	82.7	122.3	40
Fe(III)–Ce(IV) oxide	104	7 ± 0.1	7 ± 0.1	55.5	86.3	41
chestnut-like Fe_2O_3	143.12	4		137.5		42
γ-Fe_2O_3 CHNs	96.44	4		101.4		4
hollow nestlike α-Fe_2O_3	152.42			75.3		43
nano-$Mg_{0.27}Fe_{2.50}O_4$	438.2	~7	~7	83.2	127.4	44

adsorption process was time dependent. The sorption of As(V) and As(III) was rapid in the first 30 min. Thereafter it proceeded at a relatively slower rate and finally reached equilibrium after ~180 and ~240 min, respectively, for As(V) and As(III). The initial adsorption was rapid, which may be attributable to the abundant active sites on the exterior surface. Along with the increasing adsorption time, the adsorption rate gradually reduced which may be due to (i) the accumulation of adsorbed anions on the surface sites of the adsorbent; (ii) the arsenic in the solution began to diffuse into the large amounts of mesopores or micropores in the adsorbent, leading to an increasing in the diffusion resistance. Moreover, NH-ICA05 exhibited the removal efficiencies of 97.6% and 92.7%, respectively, for As(V) and As(III). The higher removal for As(V) than for As(III) is due to their different adsorption behaviors mentioned in the isotherm study. The above kinetic experimental data were fitted to the pseudo-second-order kinetic model, as presented in our previous work.[35] The estimated kinetic parameters are presented in Table S2 in the Supporting Information. The result indicates the adsorption of As(V) and As(III) can be well fitted by the pseudo-second-order kinetic model, suggesting the prevailing mechanism of the adsorption process was chemisorption. The higher k_2 for As(V) under the experimental conditions indicates the NH-ICA05 removes As(V) faster than As(III).

The removal efficiency of As(V) and As(III) by NH-ICA05 as a function of pH ranging from 2 to 10 is represented in Figure 5b. The results reveal that both As(V) and As(III) can be effectively removed by NH-ICA05 under a broad pH range from 4 to 8. The low removal efficiencies of As(V)/As(III) at pH below 4 may be due to some degree of the adsorbent dissolution. This disadvantageous condition for As(V) removal would be obvious at an alkaline condition due to the possible competition between OH^- and As(V) species. When the pH value is above 9.2, H_3AsO_3 becomes highly ionized.[37] Therefore, the decrease in As(III) removal at pH above 9 may be due to the occurrence of competitive adsorption between As(V)/As(III) species and OH^- anions. The As(III) removal efficiency almost kept at a constant level at pH ranging from 4 to 8, indicating surface charge did not have an significant effect on As(III) removal under this pH range. The superior adsorption capacities and the broad adaptation pH range for both As(V) and As(III) removal indicate the synthesized NH-ICA05 can be potentially used as an effective adsorbent for the decontamination of arsenic from water.

Competition between anions in natural water, especially oxyanions, and arsenic species for the available surface sites often occurs because of their similar anionic nature with arsenic anions. As shown in Figure 6, the coexisting NO_3^-, SO_4^{2-}, CO_3^{2-}, and F^- caused little influence on arsenic adsorption by NH-ICA05. As expected, the coexisting PO_4^{3-} exhibited the greatest influence on As(V) and As(III) adsorption capacities of NH-ICA05 followed by SiO_3^{2-}, which can be explained by the similar tetrahedral structure of arsenate, phosphate, and silicate resulting in their competitive adsorption.

3.3. Adsorption Mechanism. To clarify the adsorption mechanism of As(V)/As(III) on NH-ICA05, we investigated the surface functional groups after arsenic adsorption by FTIR spectra, as shown in Figure 7. After As(V) adsorption, the bands at 1450, 1377, and 1077 cm^{-1} clearly weakened, which indicates the CO_3^{2-}, unidentate carbonate-like species and surface hydroxyl groups simultaneously take part in the ion-exchange process with As(V) species. The peak at 615 cm^{-1}

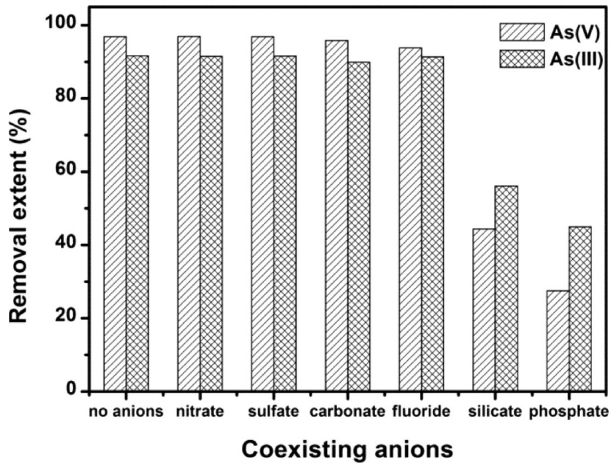

Figure 6. Effect of coexisting anions on arsenic adsorption by NH-ICA05.

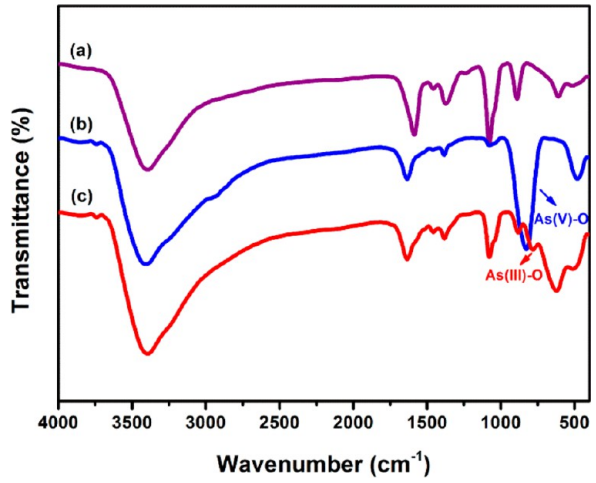

Figure 7. FTIR spectra of (a) NH-ICA05-500, NH-ICA05, (b) As(V)-loaded NH-ICA05, and (c) As(III)-loaded NH-ICA05.

also weakened, which might result from the overlapping adsorbed As(V) species. For As(III) adsorption, the intensity of the stretching vibrations of CO_3^{2-}, unidentate carbonate-like species and surface hydroxyl groups slightly changed, which implies that the ion-exchange process is not involved in the As(III) adsorption by NH-ICA05. In addition, there appears a new peak at about 830 and 790 cm^{-1} for NH-ICA05 after As(V) and As(III) adsorption, respectively. These two peaks both should be attributed to the stretching vibrations of As–O.[38,45]

Surface states of NH-ICA05 before and after arsenic adsorption were analyzed by XPS to obtain further insights into the adsorption mechanism. The XPS survey spectra revealed the existence of adsorbed arsenic species (Figure 8a). As shown in Figure S2 in the Supporting Information, in NH-ICA05, Fe existed as Fe(III) while Ce existed mostly as Ce(III) with very little Ce(IV), and the valence state of Fe and Ce changed little after adsorption for both As(V) and As(III). It indicates that there is no redox reaction occurring during the adsorption process. After As(V) adsorption, the As 3d peak located at 45.1 eV (see Figure S3a in the Supporting Information), corresponding to As(V)-O bonding, while after As(III) adsorption, the As 3d peak appeared at 44.1 eV, corresponding to As(III)-O bonding (see Figure S3b in the

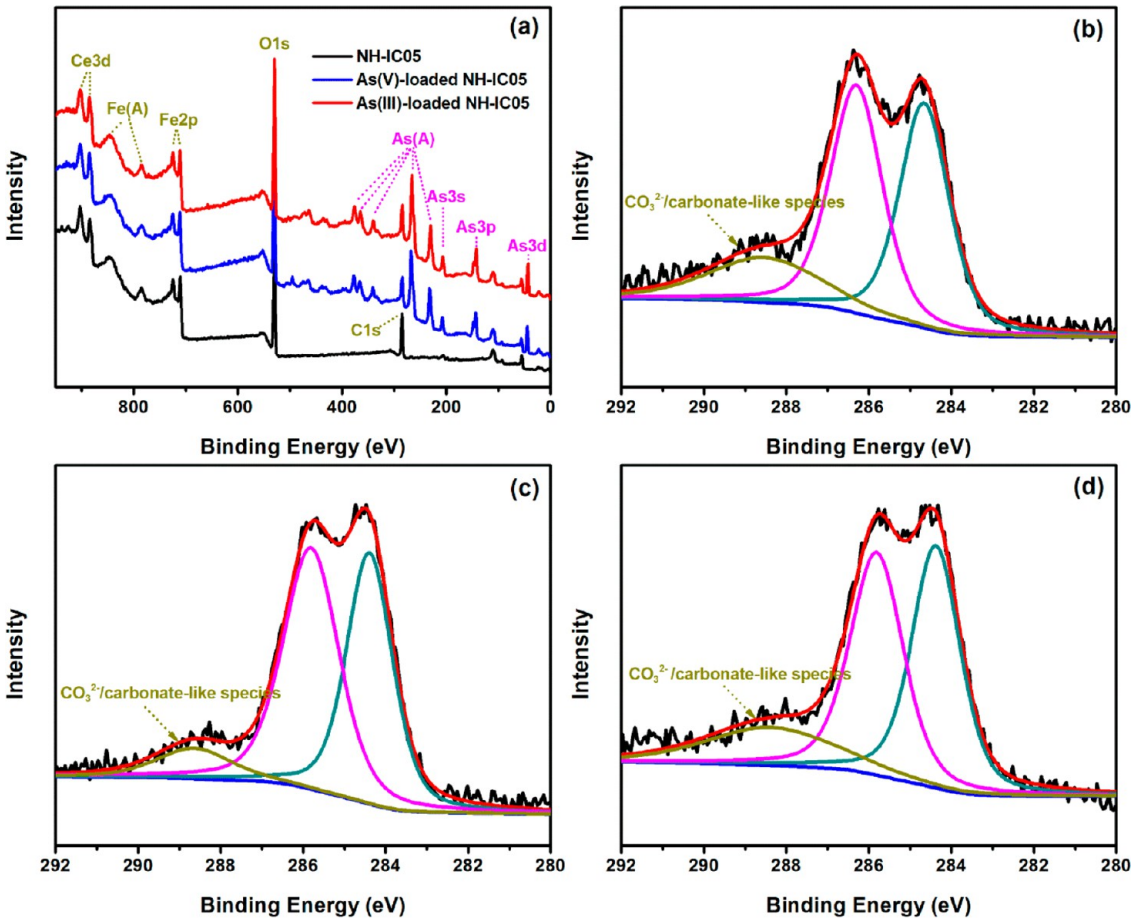

Figure 8. (a) Full-range XPS spectra of NH-ICA05 before and after arsenic adsorption, (b) C 1s spectra of NH-ICA05, (c) As(V)-loaded NH-ICA05, and (d) As(III)-loaded NH-ICA05.

Supporting Information).[46−48] The related atomic contents before and after arsenic adsorption are listed in Table 3. After

Table 3. Surface Elemental Composition of NH-ICA05 Before and After Arsenic Adsorption

samples	C (at %)	O (at %)	Ce (at %)	Fe (at %)	As (at %)
NH-ICA05	32.95	44.15	4.22	18.68	0
As(V)-loaded NH-ICA05	24.87	51.10	3.53	10.71	9.79
As(III)-loaded NH-ICA05	32.39	44.93	2.10	9.16	11.43

As(V) adsorption, the C content obviously decreased by 8.08 atom %, which is smaller than the detected As content of 9.79 atom %. This further confirmed that the CO_3^{2-} groups and unidentate carbonate-like species were replaced by As(V) species and surface hydroxyl groups might be simultaneously involved in the ion-exchange process. Differently, the C content slightly changed after As(III) adsorption, confirming that the CO_3^{2-} groups and unidentate carbonate-like species did not participate in the As(III) adsorption on NH-ICA05. Both the Fe and the Ce contents decreased after As(V)/As(III) adsorption, implying both Fe and Ce atoms were overlaid by the adsorbed As(V)/As(III) species. The atomic ratio of O increased after adsorption from 44.15% to 51.10% and 44.93%, respectively, for As(V) and As(III), which may be attributable to the introduction of As(V)/As(III) species on the surface.

The O 1s spectra of NH-ICA05 before and after arsenic adsorption are illustrated inFigure S4 in the Supporting Information. It can be clearly found that the O 1s spectra are quite different after arsenic adsorption, indicating that the oxygen constituents of NH-ICA05 significantly changed after adsorption. The O 1s narrow scans can be deconvoluted into three overlapped peaks corresponding to oxide oxygen (M-O), hydroxyl groups (OH^-) and CO_3^{2-}/carbonate-like species. The binding energy of O 1s and their variations before and after arsenic adsorption are presented in Table S3 in the Supporting Information. The M-O content increased after As(V)/As(III) adsorption, which is possibly due to (i) the formation of M−O on the surface after the reaction between adsorbents and adsorbates; (ii) the As−O in the As(V)/As(III) species. The OH^- group, which was proven to play an important role in As(V) adsorption by FTIR analysis, decreased from 54.23% to 40.18% in terms of the total oxygen.[49] The total content of CO_3^{2-} and carbonate-like species also decreased from 23.59% to 17.69%. On the contrary, the intensity of OH- and CO_3^{2-}/carbonate-like species peaks changed slightly after As(III) adsorption. The C 1s spectra before and after arsenic adsorption are presented in Figure 8. The peak at about 288.5 eV can be assigned to CO_3^{2-}/carbonate-like species.[20,21,26] The result demonstrated again that the content of CO_3^{2-}/carbonate-like species decreased after As(V) adsorption while it did not obviously change after As(III) adsorption (see Table S4 in the Supporting Information). In addition, the pH_{zpc} analysis showed that the pH_{zpc} decreased from 7.51 to 6.27 and

5.68 (see Figure S5 in the Supporting Information), respectively, after As(V) and As(III) adsorption, indicating the possible formation of the negatively charged inner-sphere complexes.[45]

Based on the above analysis, we can speculate a new As(V) adsorption mechanism involving ion-exchange between As(V) species and three types of negatively charged groups, including surface hydroxyl groups, CO_3^{2-} and unidentate carbonate-like species. Thus, the only slightly enhanced As(V) adsorption capacities by NH-ICAs result from their similar surface properties compared with IA. For As(III) adsorption, a significant increase in the adsorption capacity is predominantly attributed to the nanostructured hollow architectures of the adsorbents, which result in a large specific surface area and a porous microstructure. The main mechanism of As(III) adsorption by NH-ICA05 was possibly through surface complexing between As(III) species and surface hydroxyl groups and might even carbonate groups.

4. CONCLUSIONS

In summary, 3D hierarchical structured iron alkoxides have been synthesized by an EG mediated solvothermal method. Cerium ion doping had a significant effect on the morphology and microstructure of iron alkoxides, resulting in the significant increase in the surface area and pore volume. The relative amount of cerium ions could obviously influence the "hollowness" of the iron−cerium alkoxides. When the ratio of Fe to Ce ions was 5:1 (NH-ICA05), the product with the highest surface area and pore volume of 271.5 $m^2\ g^{-1}$ and 0.262 cc g^{-1} contains uniform particles with noticeable uniform nanostructured hollow architectures. The obtained iron−cerium alkoxides exhibit a slightly enhanced As(V) adsorption capacity compared with iron alkoxides, whereas significant enhancement for As(III) adsorption was observed. The NH-ICA05 showed the best adsorption performance with the maximum capacities of 206.6 and 266.0 mg g^{-1} for As(V) and As(III), respectively, which may be attributable to the synergistic effect of its abundant surface functional groups and the large number of uniform hollow architectures. We speculate a new mechanism for As(V) adsorption involving ion-exchange between As(V) species and surface functional groups. However, for As(III) adsorption, surface complexing is proposed. The nanostructured hollow iron−cerium alkoxide with superior adsorption capacities and broad adaptation pH ranges for both As(V) and As(III) removal indicates a great potential of this novel material as an effective adsorbent for the decontamination of arsenic from water.

■ ASSOCIATED CONTENT

Supporting Information

TGA-DSC curves of iron alkoxide; As 3d spectra of NH-ICA05 before and after arsenic adsorption; O 1s spectra of NH-ICA05 before and after arsenic adsorption; Langmuir and Freundlich isotherm parameters; the estimated kinetic parameters; relative amounts of O 1s in different chemical states; relative amounts of C 1s in different chemical states. This material is available free of charge via the Internet at http://pubs.acs.org/.

■ AUTHOR INFORMATION

Corresponding Authors

*E-mail: zzl@tongji.edu.cn. Tel: +86-21-65982426. Fax: +86-21-65984626.

*E-mail: jhchen@uwm.edu. Tel: +1-414-229-2615. Fax: +1-414-229-6958.

Notes

The authors declare no competing financial interest.

■ ACKNOWLEDGMENTS

This work was supported by the National Natural Science Foundation of China (41372241, 41072173) and State Key Laboratory of Pollution Control and Resource Reuse Foundation (PCRRK09006, PCRRY11009).

■ REFERENCES

(1) Babel, S.; Kurniawan, T. A. Low-Cost Adsorbents for Heavy Metals Uptake from Contaminated Water: A Review. *J. Hazard. Mater.* **2003**, *97*, 219−243.

(2) Hua, M.; Zhang, S.; Pan, B.; Zhang, W.; Lv, L.; Zhang, Q. Heavy Metal Removal from Water/Wastewater by Nanosized Metal Oxides: A Review. *J. Hazard. Mater.* **2012**, *211−212*, 317−331.

(3) Mohan, D.; Pittman, C. U. Arsenic Removal from Water/Wastewater Using Adsorbents-a Critical Review. *J. Hazard. Mater.* **2007**, *142*, 1−53.

(4) Mou, F.; Guan, J.; Ma, H.; Xu, L.; Shi, W. Magnetic Iron Oxide Chestnutlike Hierarchical Nanostructures: Preparation and Their Excellent Arsenic Removal Capabilities. *ACS Appl. Mater. Interfaces* **2012**, *4*, 3987−3993.

(5) Yu, X.-Y.; Xu, R.-X.; Gao, C.; Luo, T.; Jia, Y.; Liu, J.-H.; Huang, X.-J. Novel 3D Hierarchical Cotton-Candy-Like CuO: Surfactant-Free Solvothermal Synthesis and Application in As(III) Removal. *ACS Appl. Mater. Interfaces* **2012**, *4*, 1954−1962.

(6) Chen, B.; Zhu, Z.; Ma, J.; Qiu, Y.; Chen, J. Surfactant Assisted Ce-Fe Mixed Oxide Decorated Multiwalled Carbon Nanotubes and Their Arsenic Adsorption Performance. *J. Mater. Chem. A* **2013**, *1*, 11355−11367.

(7) Wu, X.-L.; Wang, L.; Chen, C.-L.; Xu, A.-W.; Wang, X.-K. Water-Dispersible Magnetite-Graphene-LDH Composites for Efficient Arsenate Removal. *J. Mater. Chem.* **2011**, *21*, 17353−17359.

(8) Carabante, I.; Grahn, M.; Holmgren, A.; Kumpiene, J.; Hedlund, J. Influence of Zn(II) on the Adsorption of Arsenate onto Ferrihydrite. *Environ. Sci. Techonol.* **2012**, *46*, 13152−13159.

(9) Catalano, J. G.; Luo, Y.; Otemuyiwa, B. Effect of Aqueous Fe(II) on Arsenate Sorption on Goethite and Hematite. *Environ. Sci. Techonol.* **2011**, *45*, 8826−8833.

(10) Fendorf, S.; Eick, M. J.; Grossl, P.; Sparks, D. L. Arsenate and Chromate Retention Mechanisms on Goethite 0.1. Surface Structure. *Environ. Sci. Techonol.* **1997**, *31*, 315−320.

(11) Ona-Nguema, G.; Morin, G.; Juillot, F.; Calas, G.; Brown, G. E. EXAFS Analysis of Arsenite Adsorption onto Two-Line Ferrihydrite, Hematite, Goethite, and Lepidocrocite. *Environ. Sci. Techonol.* **2005**, *39*, 9147−9155.

(12) Tang, W.; Su, Y.; Li, Q.; Gao, S.; Shang, J. K. Mg-Doping: A Facile Approach to Impart Enhanced Arsenic Adsorption Performance and Easy Magnetic Separation Capability to α-Fe_2O_3 Nanoadsorbents. *J. Mater. Chem. A* **2013**, *1*, 830−836.

(13) Zhong, L. S.; Hu, J. S.; Liang, H. P.; Cao, A. M.; Song, W. G.; Wan, L. J. Self-Assembled 3D Flowerlike Iron Oxide Nanostructures and Their Application in Water Treatment. *Adv. Mater.* **2006**, *18*, 2426−2431.

(14) Zhong, L. S.; Hu, J. S.; Cao, A. M.; Liu, Q.; Song, W. G.; Wan, L. J. 3D Flowerlike Ceria Micro/Nanocomposite Structure and Its Application for Water Treatment and CO Removal. *Chem. Mater.* **2007**, *19*, 1648−1655.

(15) Larcher, D.; Sudant, G.; Patrice, R.; Tarascon, J. M. Some Insights on the Use of Polyols-Based Metal Alkoxides Powders as Precursors for Tailored Metal-Oxides Particles. *Chem. Mater.* **2003**, *15*, 3543−3551.

(16) Zhang, Y.; Yang, M.; Dou, X. M.; He, H.; Wang, D. S. Arsenate Adsorption on an Fe-Ce Bimetal Oxide Adsorbent: Role of Surface Properties. *Environ. Sci. Techonol.* **2005**, *39*, 7246−7253.
(17) Wang, Y.; Morin, G.; Ona-Nguema, G.; Juillot, F.; Guyot, F.; Calas, G.; Brown, G. E., Jr Evidence for Different Surface Speciation of Arsenite and Arsenate on Green Rust: An EXAFS and XANES Study. *Environ. Sci. Techonol.* **2009**, *44*, 109−115.
(18) Farquhar, M. L.; Charnock, J. M.; Livens, F. R.; Vaughan, D. J. Mechanisms of Arsenic Uptake from Aqueous Solution by Interaction with Goethite, Lepidocrocite, Mackinawite, and Pyrite: An X-Ray Absorption Spectroscopy Study. *Environ. Sci. Techonol.* **2002**, *36*, 1757−1762.
(19) Jang, J. H.; Dempsey, B. A. Coadsorption of Arsenic(III) and Arsenic(V) onto Hydrous Ferric Oxide: Effects on Abiotic Oxidation of Arsenic(III), Extraction Efficiency, and Model Accuracy. *Environ. Sci. Techonol.* **2008**, *42*, 2893−2898.
(20) Cao, C.-Y.; Li, P.; Qu, J.; Dou, Z.-F.; Yan, W.-S.; Zhu, J.-F.; Wu, Z.-Y.; Song, W.-G. High Adsorption Capacity and the Key Role of Carbonate Groups for Heavy Metal Ion Removal by Basic Aluminum Carbonate Porous Nanospheres. *J. Mater. Chem.* **2012**, *22*, 19898−19903.
(21) Jia, Y.; Luo, T.; Yu, X. Y.; Liu, J. H.; Huang, X. J. Surfactant-Free Preparation of Nickel Carbonate Hydroxide in Aqueous Solution and Its Toxic Ion-Exchange Properties. *New J. Chem.* **2013**, *37*, 534−539.
(22) Cao, A. M.; Monnell, J. D.; Matranga, C.; Wu, J. M.; Cao, L. L.; Gao, D. Hierarchical Nanostructured Copper Oxide and Its Application in Arsenic Removal. *J. Phys. Chem. C* **2007**, *111*, 18624−18628.
(23) Poul, L.; Jouini, N.; Fiévet, F. Layered Hydroxide Metal Acetates (Metal = Zinc, Cobalt, and Nickel): Elaboration Via Hydrolysis in Polyol Medium and Comparative Study. *Chem. Mater.* **2000**, *12*, 3123−3132.
(24) Wang, Y. L.; Jiang, X. C.; Xia, Y. N. A Solution-Phase, Precursor Route to Polycrystalline SnO_2 Nanowires That Can Be Used for Gas Sensing under Ambient Conditions. *J. Am. Chem. Soc.* **2003**, *125*, 16176−16177.
(25) Jiang, X. C.; Wang, Y. L.; Herricks, T.; Xia, Y. N. Ethylene Glycol-Mediated Synthesis of Metal Oxide Nanowires. *J. Mater. Chem.* **2004**, *14*, 695−703.
(26) Cerruti, M.; Bianchi, C. L.; Bonino, F.; Damin, A.; Perardi, A.; Morterra, C. Surface Modifications of Bioglass Immersed in Tris-Buffered Solution. A Multitechnical Spectroscopic Study. *J. Phys. Chem. B* **2005**, *109*, 14496−14505.
(27) Chaudhari, N. K.; Kim, H. C.; Son, D.; Yu, J. S. Easy Synthesis and Characterization of Single-Crystalline Hexagonal Prism-Shaped Hematite Alpha-Fe_2O_3 in Aqueous Media. *CrystEngComm* **2009**, *11*, 2264−2267.
(28) Klissurski, D.; Uzunova, E. Synthesis of Nickel Cobaltite Spinel from Coprecipitated Nickel-Cobalt Hydroxide Carbonate. *Chem. Mater.* **1991**, *3*, 1060−1063.
(29) Jia, Y.; Yu, X. Y.; Luo, T.; Zhang, M. Y.; Liu, J. H.; Huang, X. J. Two-Step Self-Assembly of Iron Oxide into Three-Dimensional Hollow Magnetic Porous Microspheres and Their Toxic Ion Adsorption Mechanism. *Dalton Trans.* **2013**, *42*, 1921−1928.
(30) Burda, C.; Chen, X. B.; Narayanan, R.; El-Sayed, M. A. Chemistry and Properties of Nanocrystals of Different Shapes. *Chem. Rev.* **2005**, *105*, 1025−1102.
(31) Penn, R. L. Kinetics of Oriented Aggregation. *J. Phys. Chem. B* **2004**, *108*, 12707−12712.
(32) Politi, Y.; Arad, T.; Klein, E.; Weiner, S.; Addadi, L. Sea Urchin Spine Calcite Forms Via a Transient Amorphous Calcium Carbonate Phase. *Science* **2004**, *306*, 1161−1164.
(33) Colfen, H.; Antonietti, M. Mesocrystals: Inorganic Superstructures Made by Highly Parallel Crystallization and Controlled Alignment. *Angew. Chem., Int. Ed.* **2005**, *44*, 5576−5591.
(34) Cao, C.-Y.; Cui, Z.-M.; Chen, C.-Q.; Song, W.-G.; Cai, W. Ceria Hollow Nanospheres Produced by a Template-Free Microwave-Assisted Hydrothermal Method for Heavy Metal Ion Removal and Catalysis. *J. Phys. Chem. C* **2010**, *114*, 9865−9870.
(35) Chen, B.; Zhu, Z. L.; Guo, Y. W.; Qiu, Y. L.; Zhao, J. F. Facile Synthesis of Mesoporous Ce-Fe Bimetal Oxide and Its Enhanced Adsorption of Arsenate from Aqueous Solutions. *J. Colloid Interface Sci.* **2013**, *398*, 142−151.
(36) Wang, T.; Zhang, L. Y.; Wang, H. Y.; Yang, W. C.; Fu, Y. C.; Zhou, W. L.; Yu, W. T.; Xiang, K. S.; Su, Z.; Dai, S.; Chai, L. Y. Controllable Synthesis of Hierarchical Porous Fe_3O_4 Particles Mediated by Poly(Diallyldimethylammonium Chloride) and Their Application in Arsenic Removal. *ACS Appl. Mater. Interfaces* **2013**, *5*, 12449−12459.
(37) Ben Issa, N.; Rajakovic-Ognjanovic, V. N.; Jovanovic, B. M.; Rajakovic, L. V. Determination of Inorganic Arsenic Species in Natural Waters-Benefits of Separation and Preconcentration on Ion Exchange and Hybrid Resins. *Anal. Chim. Acta* **2010**, *673*, 185−193.
(38) Yu, X. Y.; Luo, T.; Jia, Y.; Zhang, Y. X.; Liu, J. H.; Huang, X. J. Porous Hierarchically Micro-/Nanostructured MgO: Morphology Control and Their Excellent Performance in As(III) and As(V) Removal. *J. Phys. Chem. C* **2011**, *115*, 22242−22250.
(39) Zhang, G.; Qu, J.; Liu, H.; Liu, R.; Wu, R. Preparation and Evaluation of a Novel Fe-Mn Binary Oxide Adsorbent for Effective Arsenite Removal. *Water Res.* **2007**, *41*, 1921−1928.
(40) Zhang, G.; Ren, Z.; Zhang, X.; Chen, J. Nanostructured Iron(III)-Copper(II) Binary Oxide: A Novel Adsorbent for Enhanced Arsenic Removal from Aqueous Solutions. *Water Res.* **2013**, *47*, 4022−4031.
(41) Basu, T.; Nandi, D.; Sen, P.; Ghosh, U. C. Equilibrium Modeling of As(III,V) Sorption in the Absence/Presence of Some Groundwater Occurring Ions by Iron(III)-Cerium(IV) Oxide Nanoparticle Agglomerates: A Mechanistic Approach of Surface Interaction. *Chem. Eng. J.* **2013**, *228*, 665−678.
(42) Mou, F. Z.; Guan, J. G.; Xiao, Z. D.; Sun, Z. G.; Shi, W. D.; Fan, X. A. Solvent-Mediated Synthesis of Magnetic Fe_2O_3 Chestnut-Like Amorphous-Core/Gamma-Phase-Shell Hierarchical Nanostructures with Strong As(V) Removal Capability. *J. Mater. Chem.* **2011**, *21*, 5414−5421.
(43) Wei, Z.; Xing, R.; Zhang, X.; Liu, S.; Yu, H.; Li, P. Facile Template-Free Fabrication of Hollow Nestlike α-Fe_2O_3 Nanostructures for Water Treatment. *ACS Appl. Mater. Interfaces* **2013**, *5*, 598−604.
(44) Tang, W.; Su, Y.; Li, Q.; Gao, S.; Shang, J. K. Superparamagnetic Magnesium Ferrite Nanoadsorbent for Effective Arsenic (III, V) Removal and Easy Magnetic Separation. *Water Res.* **2013**, *47*, 3624−3634.
(45) Pena, M.; Meng, X.; Korfiatis, G. P.; Jing, C. Adsorption Mechanism of Arsenic on Nanocrystalline Titanium Dioxide. *Environ. Sci. Techonol.* **2006**, *40*, 1257−1262.
(46) Fullston, D.; Fornasiero, D.; Ralston, J. Oxidation of Synthetic and Natural Samples of Enargite and Tennantite: 2. X-Ray Photoelectron Spectroscopic Study. *Langmuir* **1999**, *15*, 4530−4536.
(47) Ouvrard, S.; De Donato, P.; Simonnot, M.; Begin, S.; Ghanbaja, J.; Alnot, M.; Duval, Y.; Lhote, F.; Barres, O.; Sardin, M. Natural Manganese Oxide: Combined Analytical Approach for Solid Characterization and Arsenic Retention. *Geochim. Cosmochim. Acta* **2005**, *69*, 2715−2724.
(48) Ma, J.; Zhu, Z.; Chen, B.; Yang, M.; Zhou, H.; Li, C.; Yu, F.; Chen, J. One-Pot, Large-Scale Synthesis of Magnetic Activated Carbon Nanotubes and Their Applications for Arsenic Removal. *J. Mater. Chem. A* **2013**, *1*, 4662−4666.
(49) Deliyanni, E.; Nalbandian, L.; Matis, K. Adsorptive Removal of Arsenites by a Nanocrystalline Hybrid Surfactant-Akaganeite Sorbent. *J. Colloid Interface Sci.* **2006**, *302*, 458−466.